High Strain-rate Dynamic Compressive Behavior and Energy Absorption of Distiller's Dried Grains and Soluble Composites with Paulownia and Pine Wood Using a Split Hopkinson Pressure Bar Technique

Damian Stoddard,[a,*] Suman Babu Ukyam,[a] Brent Tisserat,[b] Ivy Turner,[a] Rowan Baird,[a] Sofia Serafin,[a] Jose Torrado,[a] Birendra Chaudhary,[a] Alex Piazza,[a] Mason Tudor,[a] and Arunachalam M. Rajendran [a]

Novel bio-based composite wood panels (CWPs) that consisted of distiller's dried grains and solubles (DDGS) flour adhesive bound to a wood filler/reinforcement were subjected to high strain-rate compression loading, and their behavior was investigated. Specimens of DDGS-Paulownia wood (PW) or DDGS-pinewood (Pine) composites made using DDGS with fractions of 10%, 15%, 25%, and 50% were tested at high strain-rates using a modified compression Split Hopkinson Pressure Bar (SHPB). Both DDGS-PW and DDGS-Pine composites displayed strain-rate sensitivity, and DDGS-PW had a 25% fraction, which showed the highest ultimate compressive strength of 655 MPa at approximately 1600/s. The 90%-PW had the highest specific energy of 19.24 kJ/kg at approximately 1600/s when loaded *via* dynamic compression. The CWPs constructed of DDGS-PW had higher strength and energy absorption than DDGS-Pine with the exception of the 50% DDGS composites.

INTRODUCTION

By 2030, global consumption of industrial and solid wood is predicted to increase by 60% (Elias and Boucher 2014). Engineered wood products, including composite wood panels (CWPs) (*e.g.*, fiberboards, particleboard, medium density fiberboard, and high density fiberboards) are an important material in the building and furniture industries (Woodpansonline 2015; Grand View Research 2018; Displays2GO 2019). The global CWP market is valued at approximately $91 billion (Woodpansonline 2015). Composite wood panels are designed precisely as per international standards to meet the increasing demand for wood in various applications, such as domestic housing projects and industries. Currently, CWPs are composed of a matrix adhesive (typically a synthetic resin) that binds wood particles, fibers, or veneers of wood together using heat and pressure. Composite wood panels fulfill certain applications that solid wood cannot perform due to their dimensional versatility and overall isotropic strength obtained through the design process.

Composite wood panels are available in a wide variety of thicknesses, sizes, and grades to meet application-specific performance requirements.

Composite wood panels manufactured using petroleum-based resins emit volatile organic compounds, such as formaldehyde (Sawyers 2009; Grand View Research 2018). Formaldehyde is a known carcinogen and has adverse environmental and health consequences (Sawyers 2009; Grand View Research 2018). Several bio-adhesives have employed soy adhesives, which is the most common bio-adhesive employed currently; however, there are numerous alternative bio-based adhesives such as tannins, lignins, starch *etc.* (Amaral-Labat *et al.* 2008; Frihart and Birkeland 2016; Vnučec *et al.* 2016; Ghahri and Mohebby 2017; Hemmilä *et al.* 2017). Soybean flour proteins are abundant, renewable, biodegradable, and free of formaldehyde. Soy flour adhesives have high adhesion strength; however, they are more expensive than synthetic urea-formaldehyde and phenol-formaldehyde resins (Vnučec *et al.* 2016). The protein portion of the soy flour is responsible for its adhesive properties (Amaral-Labat *et al.* 2008; Frihart and Birkeland 2016; Vnučec *et al.* 2016; Ghahri and Mohebby 2017; Hemmilä *et al.* 2017). Defatted soy flour contains approximately 50% protein (Amaral-Labat *et al.* 2008; Frihart and Birkeland 2016; Ghahri and Mohebby 2017). Alternatively, distiller's dried grain and solubles (DDGS) obtained from dry mill processing is a less expensive bio-based adhesive (USGC 2017). In the United States, the main feedstock for the production of ethanol is corn. Distiller's dried grain and solubles is a byproduct of the ethanol fermentation process from corn (Pažitný et al. 2011). In 2017, approximately 90% of U.S. ethanol was produced from 214 dry grind ethanol plants. As a result, about 36.5 million metric tons of distiller's co-products were expected to be produced in 2017 (USGC 2017). Distiller's dried grain and solubles is composed of approximately 30% protein, 10% oil, and 54% carbohydrates, and it has a 10% moisture content (USGC 2017). In addition, DDGS has a long shelf life and can be shipped to locations far from the ethanol production facility.

Previously, DDGS has been employed as an inert low-cost bio-filler with phenolic resin to produce composites of high flexural strength (Cheesbrough *et al.* 2008). Tisserat *et al.* (2013b) produced plastic composites of high-density polyethylene (HDPE) matrices and reinforced them with solvent-extracted DDGS that exhibited superior tensile and flexural properties but lower impact energy properties than neat HDPE. Recently, Tisserat *et al.* (2018a, 2018b) fabricated CWPs composed of a DDGS matrix reinforced with Paulownia wood (PW). These DDGS-PW composite panels exhibited flexural and water resistance properties similar to soy flour-PW composites. In addition, the panels exhibited flexural properties that satisfy the industry standards. However, these CWPs had inferior water resistance, which suggests that their use may be limited to interior applications.

Typically, commercial CWPs are manufactured from sawn wood wastes (*i.e.*, scraps, chips, and sawdust) of various species. However, this study utilized two different wood types as reinforcement components: Paulownia (PW) (*Paulownia elongata*) and Eastern White Pine (*Pinus ponderosa*). Paulownia is a fast-growing biomass tree that will likely become a source of woody biomass in the future (Joshee 2012; Sutton 2019). Paulownia is notable because it is a lightweight hardwood (Joshee 2012; Sutton 2019). It is employed in the furniture industry due to its light weight and pale appearance that typically has minimal knots. Paulownia has also been employed to manufacture wood-plastic composites that are relatively light but exhibit strong reinforcement properties (Tisserat *et al.* 2013a,c). The eastern white pine is a lumber tree grown throughout the north-eastern regions of the US and Canada (Wendel and Smith 1990; ACS 2019).

In many structural applications, engineered wood composites are subjected to dynamic loading conditions. The energy absorption and dissipation capabilities of composites are important during impact events. Thus, a detailed understanding of the dynamic behavior and energy absorption characteristics of engineered wood composites is warranted.

The Split Hopkinson Pressure Bar (SHPB) experimental technique has often been used to evaluate fiber-reinforced composites at high strain-rates. Allazadeh and Wosu (2011) reported the dynamic response of dry maple wood under a high strain-rate compressive loading using an SHPB. Results indicated that the damage mode was dependent on the incident energy, strain-rate, geometrical dimensions, and material structure. Widehammar (2004) performed dynamic tests to study the stress-strain relationships for spruce wood, and he established that wood behavior is greatly influenced by strain-rate, moisture content, and loading direction. In this study, the dynamic compression tests were performed on DDGS-PW and DDGS-Pine (Pine wood) wood composite specimens on a modified SHPB to determine the strain-rate sensitivity and ultimate compressive strength.

EXPERIMENTAL

Materials and Methods

The DDGS employed is marketed as a commercial animal corn feed pellet product, and it was procured from Archers Daniel Midland Co. (Chicago, IL, USA). Pine wood shavings were obtained from commercially sold pet bedding (Petsmart, Phoenix, AZ, USA). Paulownia wood was harvested from 36-month-old trees grown in Fort Valley, GA (Fort Valley State University, Fort Valley, GA, USA) and were then shipped to the USDA-NCAUR laboratory for processing. First, the paulownia was chipped several times through a chipper to obtain suitable shavings. Pine wood and PW were then milled using a Model 4 Thomas-Wiley mill grinder (Thomas Scientific, Swedesboro, NJ, USA) to reduce their size. Sizing of PW and Pine wood particles was conducted with a Ro-Tap^{Tm} Shaker (Model RX-29; W.S Tyler, Mentor, OH, USA) to obtain one particle size selection of ≤ 600 µm and another size selection of 600 µm to 1700 µm particles. The PW and Pine contained approximately 6% moisture. The DDGS was first ground in a Wiley mill using a 2-mm opening sieve to obtain fine particles, and it was then defatted with hexane using a Soxhlet extractor. Defatted DDGS contained 30% crude protein and 5% moisture. The DDGS was ground into a flour consistency using a laboratory grinder (Ririhong Model RRA-500, Shanghai Yuanwo Industrial and Trade Company, Shanghai, China) and sieved to obtain particles of ≤ 250 µm.

Theory/Analysis

The DDGS-PW and DDGS-Pine composites were fabricated with 10% to 50% DDGS and paulownia or pinewood through a phase change process. The DDGS reacted with PW or Pine particles under high pressure and temperature to become a "liquid-gel" matrix and interfacial bond to the wood to produce CWPs, as shown in Fig. 1. Four different 10-mm-thick particleboards were constructed for each wood constituent type: 10% DDGS-90% wood; 15% DDGS-85% wood, 25% DDGS-75% wood, and 50% DDGS-50% wood. Samples of each variant with dimensions of 10 mm × 10 mm × 10 mm were prepared to maintain an aspect ratio of 1 for SHPB testing.
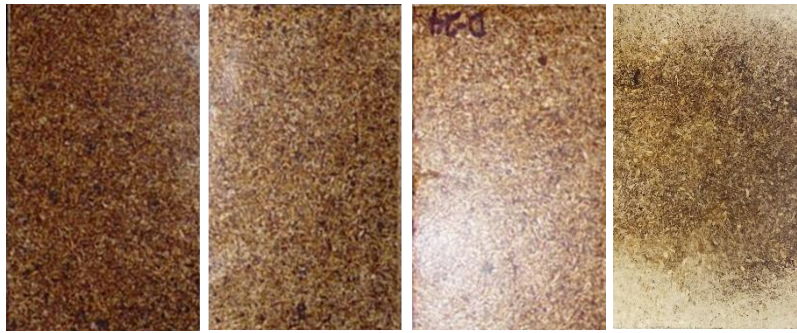
Fig 1. Particleboards constructed of wood and DDGS

The CWPs were conditioned at 25 °C and 50% relative humidity (RH) for 72 h prior to flexural testing. Using a table saw, panels were cut into suitable specimen boards to administer the three-point bending tests as per EN 310 (1993). For each formulation, five specimen panels were tested. Specimen thickness dictates the free span length used to conduct flexural tests with the Instron Model 1122 universal testing machine (Instron Corp., Norwood, MA, USA). The compression SHPB technique utilizes a striker bar to generate a compressive stress wave (incident wave) that travels through the incident bar. The incident wave propagates through the incident bar towards a sample located between the incident bar and the transmission bar. Due to a change in impedance, a portion of the incident wave is reflected and transmitted through the sample and transmission bar. The stress waves are captured by using strain gauges located on the incident and transmission bars shown in Fig. 2. Utilizing the stress waves allows for the high strain-rate material response to be analyzed.
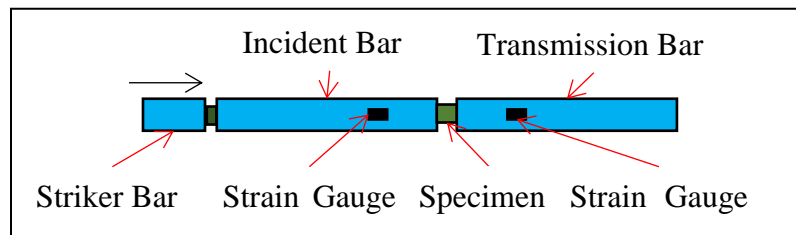

Fig. 2. The SHPB experimental setup schematic

The displacement at the end of the incident and transmission bar was determined using elastic wave theory as shown in Eqs. 1 and 2,

$$U_1 = \int_0^t C_o \varepsilon_1 dt \qquad (1)$$
$$U_2 = \int_0^t C_o \varepsilon_2 dt \qquad (2)$$

where C_o is the elastic wave speed (mm/s) and ε_1 and ε_2 are the strain in the incident bar and transmission bar, respectively. The elastic wave speed can be calculated as follows,

$$C_o = \sqrt{\frac{E}{\rho}} \qquad (3)$$

where E is the elastic modulus of the bar (MPa), and ρ is the density of the bar (kg/mm^3).

Using the incident, reflected, and transmission strain, the displacement at the end of the incident bar can be displayed in terms of the incident, reflected, and transmission

strain, as shown in Eqs. 4 and 5,

$$U_1 = C_o \int_0^t (\varepsilon_i - \varepsilon_r) dt \qquad (4)$$

$$U_2 = C_o \int_0^t \varepsilon_t dt \qquad (5)$$

where ε_i, ε_r, and ε_t are the incident strain voltage for the incident, reflected, and transmitted wave, respectively, and t is time (s). Utilization of the displacement at the ends of the bar allowed for the sample strain to be obtained with Eq. 6,

$$\varepsilon_s = \frac{U_1 - U_2}{L_s} \qquad (6)$$

where L_s is the length (mm) of the sample.

Combining Eqs. 4 and 5 into Eq. 6 gives the relationship between the incident, reflected, and transmission strain with the sample strain (Eq. 7):

$$\varepsilon_s = \frac{C_o}{L_s} \int_0^t (\varepsilon_i - \varepsilon_r - \varepsilon_t) dt \qquad (7)$$

The force at each end of the sample must be equal to maintain stress equilibrium within the sample. The force at each end of the sample can be obtained using Eqs. 8 and 9,

$$P_1 = E_b A_b (\varepsilon_i + \varepsilon_r) \qquad (8)$$

$$P_2 = E_b A_b \varepsilon_t \qquad (9)$$

where E_b, A_b are the modulus (MPa) and area (mm^2) of the bar, respectively.

Setting P_1 equal to P_2 and simplifying yields the equilibrium condition used to validate the dynamic compression loading during the SHPB technique, (Eq. 10):

$$\varepsilon_i + \varepsilon_r = \varepsilon_t \qquad (10)$$

Simplifying Eq. 7 using Eq. 10 allows the sample strain to be expressed in terms of the reflected strain (Eq. 11) and can also be used to obtain the strain-rate at any time (Eq. 12):

$$\varepsilon_s = \frac{-2C_o}{L_s} \int_0^t \varepsilon_r dt \qquad (11)$$

$$\dot{\varepsilon}_s = \frac{-2C_o}{L_s} \varepsilon_r(t) \qquad (12)$$

Stress in the sample can be obtained from the force applied to the sample and the cross-sectional area of the bar and sample using Eq. 13:

$$\sigma_s = E_b \frac{A_b}{A_s} \varepsilon_t(t) \qquad (13)$$

Sample stress-strain curves for samples can be constructed using Eqs. 12 and 13 at a particular strain-rate. A more comprehensive explanation of the fundamental formulation of SHPB equations was given by Lang (2012).

Experimental Setup

All tests for characterizing wood samples at high strain-rates were conducted on a modified SHPB in the Blast and Impact Dynamics Lab at the University of Mississippi (Oxford, MS, USA). Aluminum bars of 19 mm diameter were used as striker, incident, and transmission bars. A pulse shaper made of copper was placed between the striker and incident bars to ramp the incident pulse to achieve stress equilibrium within the specimen. Frew *et al.* (2002) discuss the pulse shaping technique for compressive testing on SHPB in

detail. A Shimadzu HPV-2 (Shimadzu Corporation, Kyoto, Japan) high-speed video camera with a fixed resolution of 312 pixels × 260 pixels and a recording speed of 250,000 fps was used to capture the deformation/failure process. Variable pressures were used to obtain multiple strain-rates under compressive loading, and the DDGS-PW and DDGS-Pine specimens were placed between the incident and transmission bars, as shown in Fig. 3.
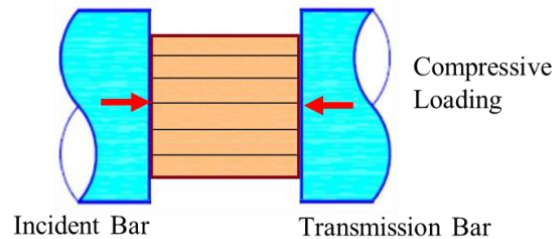

Fig. 3. Dynamic compressive loading on the DDGS-PW and DDGS-Pine specimen

RESULTS AND DISCUSSION

The SHPB high strain-rate compression tests were performed on DDGS-PW and DDGS-Pine to study their dynamic behavior and energy absorption characteristics. The required dynamic equilibrium condition was validated in all compression tests by calculating the stresses developed at the opposite surfaces of each specimen under compression using Eqs. 8 and 9. Excellent correlations between bar-end forces were observed for all samples throughout the stress pulse duration. Figure 4 shows the typical force equilibrium.
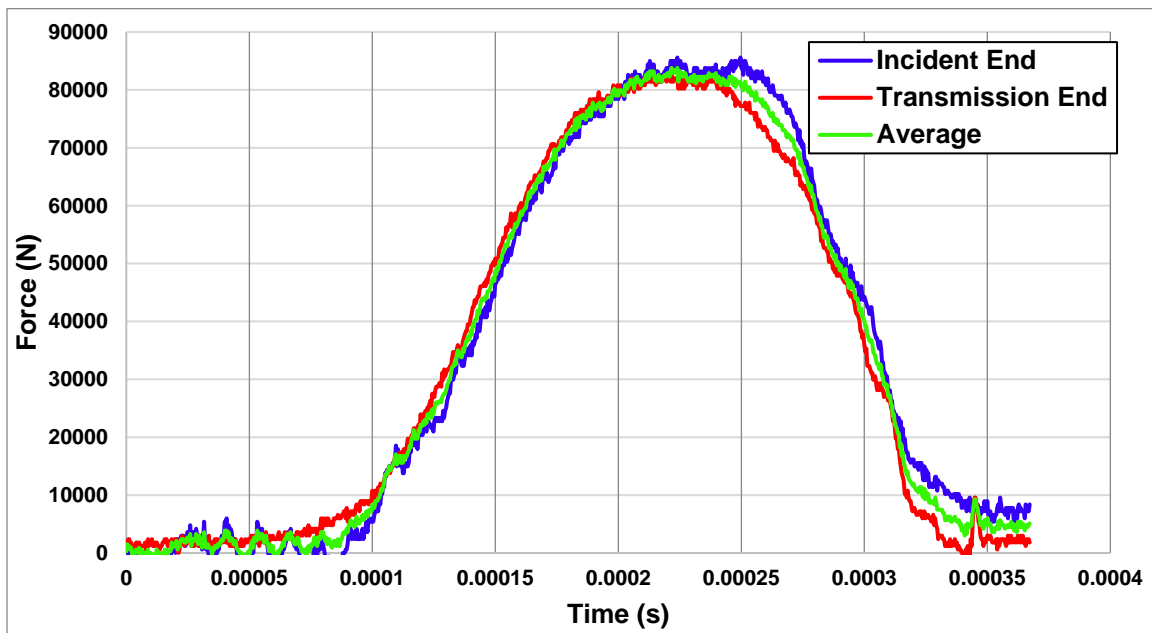

Fig. 4. Validation of dynamic stress equilibrium for the SHPB compression test of DDGS-PW specimen

bioresources.com

Secondary validation was done using the Shimadzu HPV-2 high-speed video camera to capture the sample strain under dynamic compression loading. The 1-D tracking feature in Xcitex ProAnalyst software (Xcitex Organization, Version 1.6.0.2, Cambridge, MA, USA) was used to track the change in length between the incident and transmission bar. Digital image correlation (DIC) showed an excellent correlation with the strain results obtained from conventional SHPB analysis.
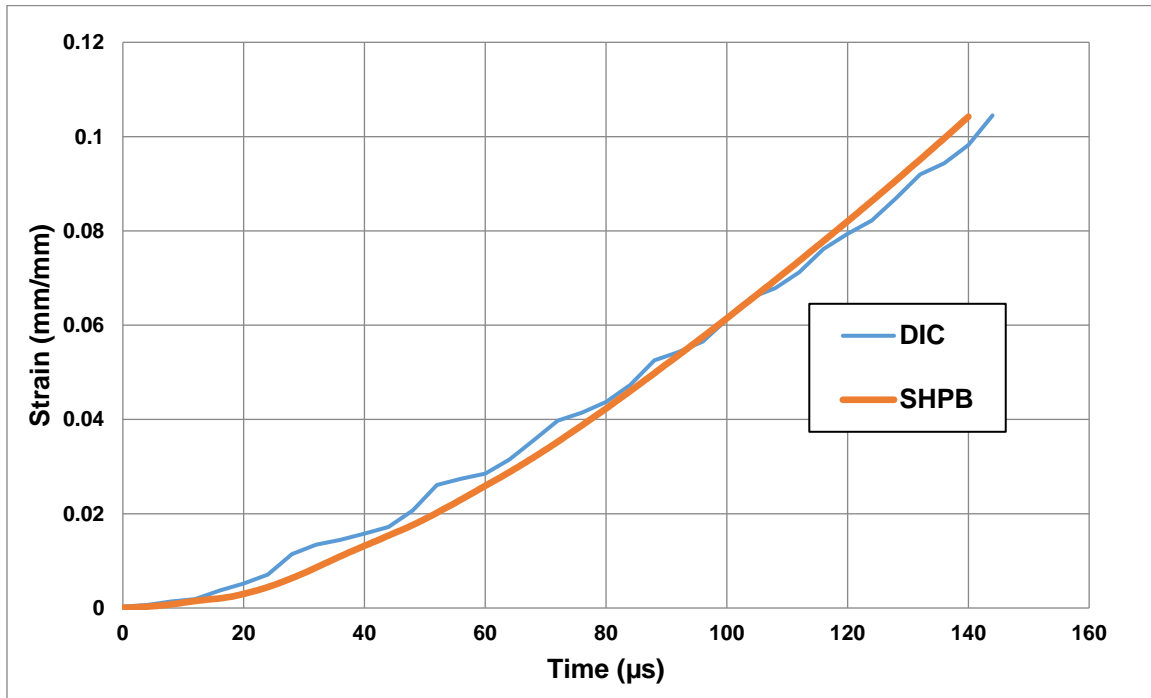

Fig. 5. The DIC validation of strain

Digital image correlation was also used to observe the failure characteristics of each sample during dynamic compression loading. Figure 6 shows high-speed images of typical high strain-rate response of DDGS wood composite when subjected to high strain-rate loading. In addition, it includes the correlation between the corresponding images with the stress-strain curve. Fracture occurred after peak load was achieved, and a rapid loss in strength was observed.

A set of five specimens from each composite variant were tested at three different strain-rates of approximately 1000/s, 1400/s, and 1600/s. Sample stress-strain curves for the compression testing of each composite variation are shown in Figs. 7a to 7h. The 90%-PW and 75%-PW (Figs. 7a and 7c, respectively) showed an initial decrease in stiffness (initial slope of stress-strain curve) when strain-rate increased from approximately 1000/s to 1400/s, and stiffness increased when strain-rate increased from approximately 1400/s to 1600/s. The decrease in stiffness was likely caused by interfacial delamination between DDGS and PW due to the low fraction of DDGS binder. The increase in stiffness from approximately 1400/s to 1600/s was likely caused by the strain-rate sensitivity of the DDGS and/or PW. More investigation is needed to obtain which of the constituent materials is the cause of the strain rate sensitivity.
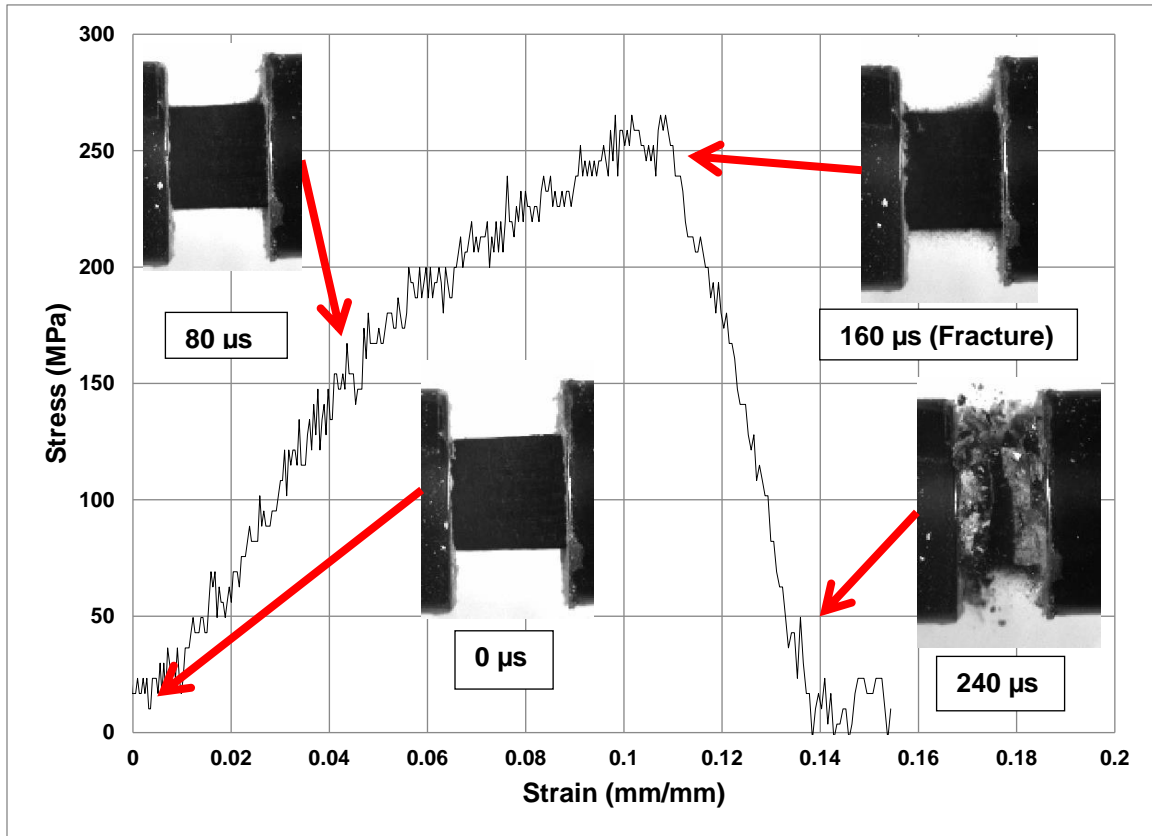
Fig. 6. High-speed digital image correlation with sample stress-strain

The 90%-PW and 75%-PW exhibited an increase in strain to failure when strain-rate increased from approximately 1000/s to 1400/s, and strain to failure decreased when strain-rate increased from approximately 1400/s to 1600/s. The initial increase in strain to failure was likely due to the lower strain-rate response being dominated by the wood and the higher strain-rate response being dominated by the DDGS and interfacial strength. A decrease in compressive strength was observed when strain-rate increased from approximately 1000/s to 1400/s, and compressive strength increased when strain-rate increased from approximately 1400/s to 1600/s for 90%-PW and 85%-PW. The variation in compressive strength was likely caused by the same mechanisms previously stated for stiffness. The 75%-PW (Fig. 7e) showed two typical responses when subjected to high strain-rate compression. The responses at approximately 1000/s and 1400/s were similar, and only slight variations consistent with composite materials were observed. The similarity of response was likely caused by the increase in fraction of DDGS, which may have caused the compressive response to be less dominated by the wood constituent material. An increase in stiffness was observed as strain-rate increased from approximately 1000/s to 1400/s to 1600/s. The increase in stiffness was likely caused by the strain-rate sensitivity of the DDGS and/or PW. A decrease in strain to failure was observed as strain-rate increased from 1000/s to 1400/s to 1600/s. The increase in dynamic properties was qualitatively consistent with the response of the 90%-PW and 85%-PW when strain-rate was increased from approximately 1400/s to 1600/s. Compressive strength increased when strain-rate was increased from approximately 1000/s to 1400/s to 1600/s. The 50%-PW (Fig. 7g) exhibited a slight increase in stiffness and strength with increasing strain-rate. Strain to failure increased as strain-rate decreased, but strength decreased. The 90%-Pine

_____ *bioresources*.com

and 75%-Pine (Figs. 7b and 7d, respectively) exhibited similar responses to high strain-rate compression loading. Both compositions showed a decrease in stiffness and strength and an increase in strain to failure as strain-rate increased. Notably, the response exhibited by the lower strain-rate shown in Figs. 7b and 7d was consistently stiffer, and the higher strain-rate gave a wide variety of responses, which ranged from the stiffest response to the softest. The 75%-Pine (Fig. 7f) showed increasing stiffness and strength as strain-rate increased, which was consistent with previously mentioned composites, and strain to failure increased as strain-rate decreased. The bonding strength likely played a major role in the strength of the composites at 25% DDGS compositions. The 50%-Pine showed no strain-rate sensitivity. This was likely caused by a specific failure mechanism in the specimen that does not allow a higher response to be exhibited. For example, the response may be limited solely by the failure mechanism, and the strain-rate stiffening previously exhibited is not able to transpire due to the failure mechanism.

Peak compressive strength and stiffness increased when DDGS-PW percentages increased from 10% to 25% at both approximately 1400/s and approximately 1600/s when comparing the same strain-rate at different DDGS percentage. This suggested that the strain-rate sensitivity and strength was due to the DDGS content and bonding strength between PW and DDGS. When the content was increased to 50%, a decrease in strength and stiffness was observed, which was likely caused by a decrease in strength due to the addition of lower strength binder (DDGS). A strain-rate of approximately 1000/s strain-rate showed an initial increase in strength as DDGS-Pine content increased from 10% to 15%, and strength decreased when DDGS-Pine content increased from 15% to 50%. These findings suggested that an ideal ratio of binder could be achieved to obtain the best properties for specific energy absorption applications. The DDGS-Pine exhibited approximately the same strength at low strain-rate when DDGS percentage was increased from 10% to 25%, and an increase in strength was seen at 50%-Pine. The middle strain-rate showed a slight decrease in strength of 10% for 85%-Pine and an increase of 15% for 75%-Pine. The peak compressive strength at 25% and 50% were approximately the same.

The 90%-PW, 85%-PW, and 75%-PW gave stiffer responses to dynamic loading than 90%-Pine, 85%-Pine, and 75%-Pine, respectively. The PW composite had higher peak strength than the Pine composites for each corresponding percentage and strain-rate. This was likely due to the differences in bonding strength between DDGS-PW and DDGS-Pine. An inverse response was observed when comparing the dynamic properties of 50%-PW and 50%-Pine. This increase in strength may have been caused by the slightly higher strain-rate achieved when testing the samples. Alternatively, it may have been due to the dynamic response being dominated more by the response of the DDGS.

Trends for the dynamic compressive strength and specific energy absorption for PW and Pine composites can be seen in Figs. 8 through 11. It was observed that the compressive strength of the PW at all strain-rates exhibited an increasing trend to a peak strength and matrix percentage and then a decrease, further validating the claim of an optimal composite design (between 15 to 25%). The specific energy for PW composites showed an overall decreasing trend in energy absorption with respect to both matrix and strain-rate with the exception of 15% at strain-rates 1400/s and 1600/s. The composite made of pine showed an increasing trend in compressive strength with increasing matrix percentage. An overall decreasing trend was observed for specific energy with increasing matrix percentage with the exception of 1400/s.
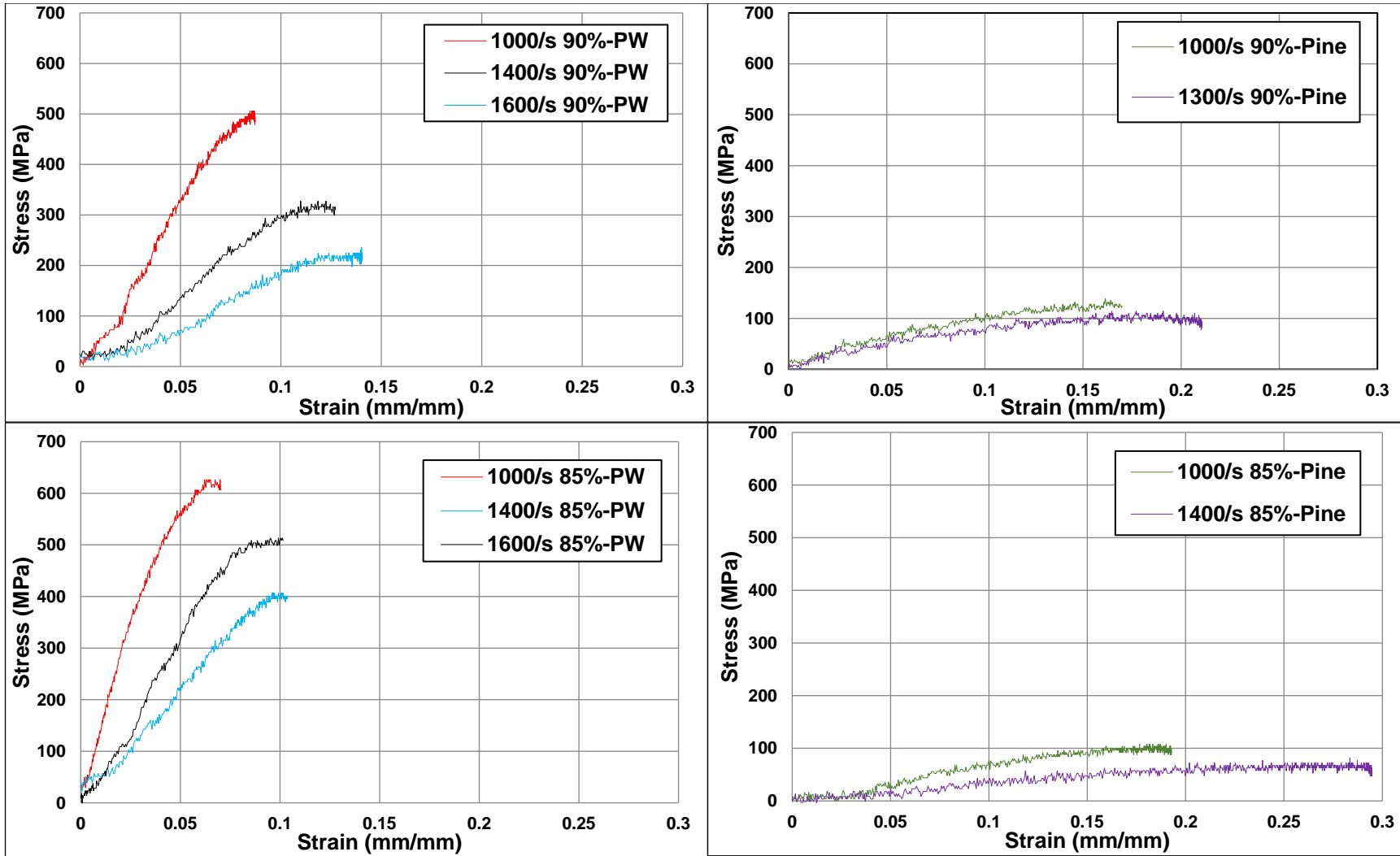
Fig. 7. a) 10% DDDS-PW, b) 10% DDGS-Pine, c) 15% DDGS-PW, d) 15% DDGS-Pine dynamic stress-strain response at various strain-rates
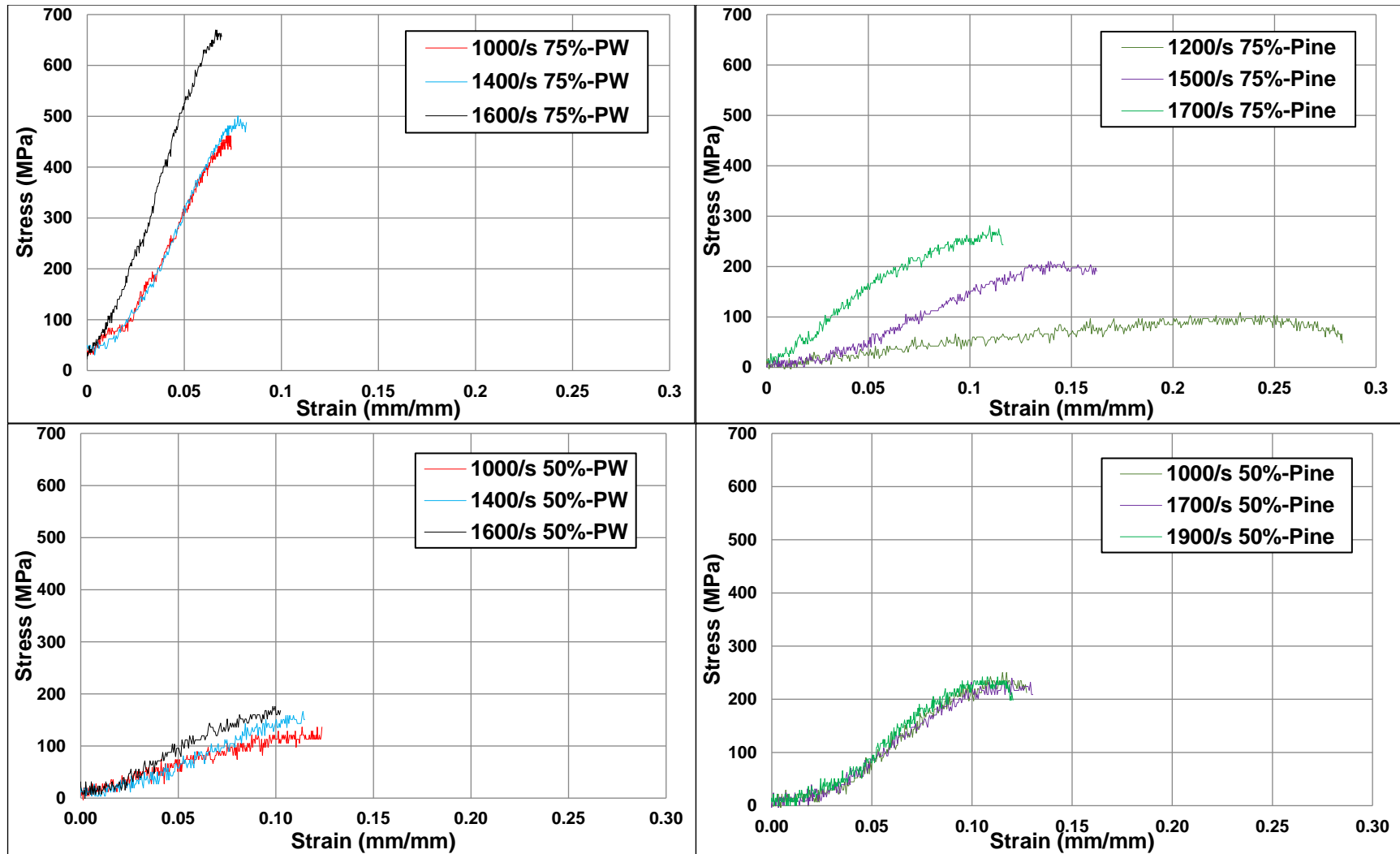
bioresources.com

Fig. 7. e) 25% DDGS-PW, f) 25% DDGS-Pine, g) 50% DDGS-PW, and h) 50% DDGS-Pine dynamic stress-strain response at various strain-rates

bioresources.com

The quasi-static flexural properties of the CWPs are given in Table 1. Generally, CWPs that contained higher matrix dosages of DDGS exhibited higher flexural properties (*i.e.,* Modulus of Rupture (MOR) and Modulus of Elasticity (MOE)). There were high correlations between the physical dimension properties (thickness and densities) and the flexural properties. This was due to the greater interfacial binding that occurred between the matrix adhesive and wood reinforcement. However, the 50%-PW CWP flexural properties did not exceed the 75%-PW CWP, which suggested that maximum matrix interfacing occurred.
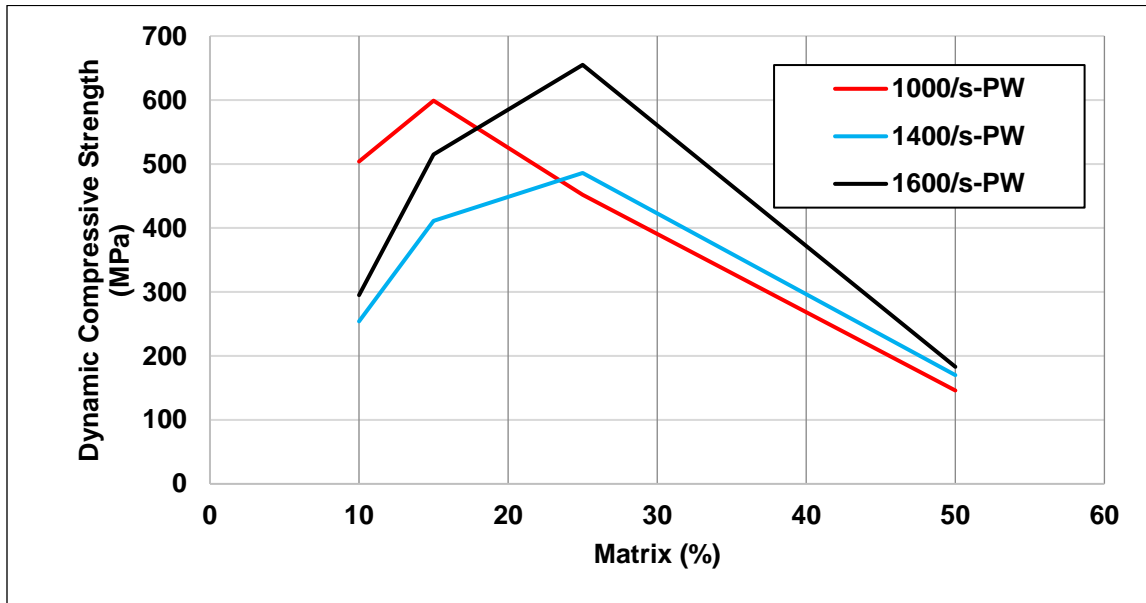

Fig. 8. Dynamic compressive strength-matrix % comparison for various strain-rates for paulownia wood composites
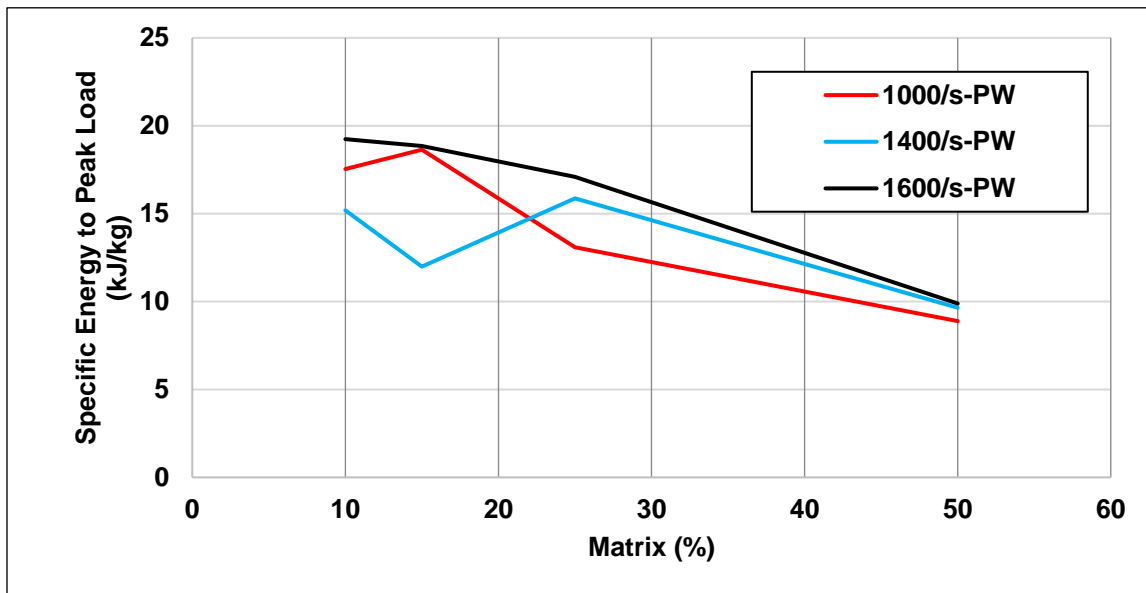

Fig. 9. Specific energy-matrix % comparison for various strain-rates for paulownia wood composites
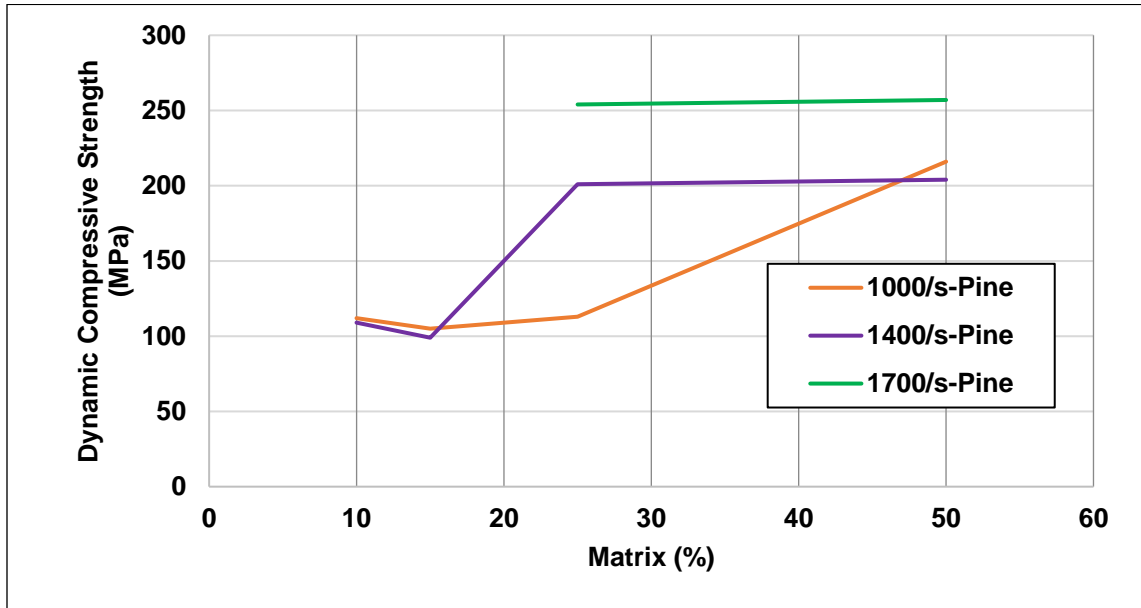
Fig. 10. Dynamic compressive strength-matrix % comparison for various strain-rates for pine wood composites
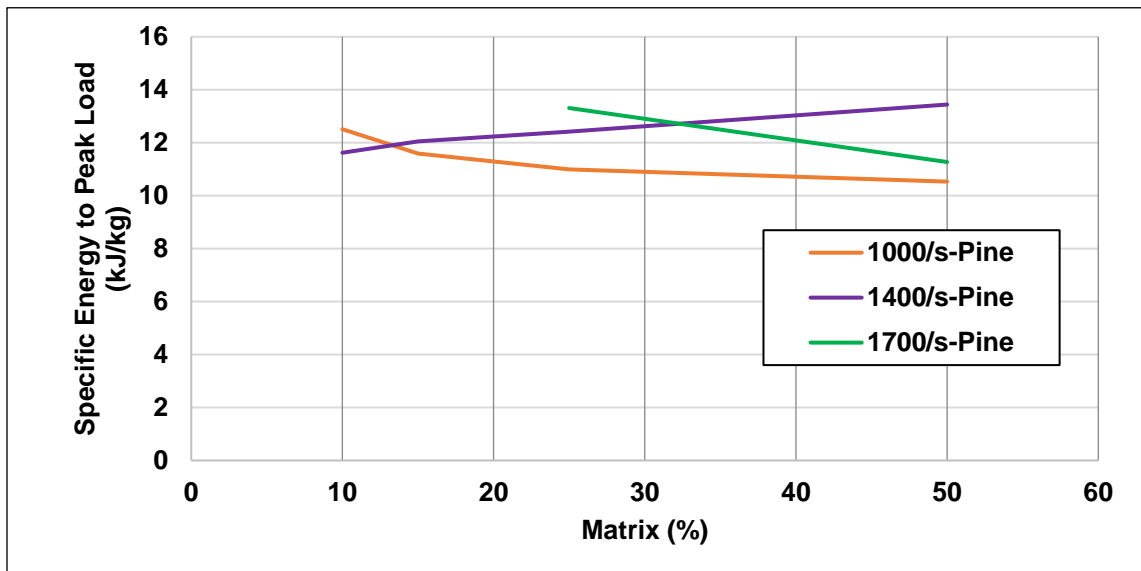
Fig. 11. Specific energy-matrix % comparison for various strain-rates for pine wood composites

The CWPs composed of DDSG-PW exhibited higher flexural properties than the CWPs composed of DDGS-Pine. This may have occurred because PW provided superior binding surfaces than those of Pine. Each wood species has its own characteristic chemistry and physical properties that influence its mechanical properties (Pettersen 1984; Olson and Carpenter 1985; Green *et al.* 1999; Rencoret *et al.* 2009; Yang and Jaakkola 2011; Kirker *et al.* 2013; Tsoumis 2019). There were several high correlations between the flexural properties, resin dosages, and the ultimate compressive strength and specific energy to peak load (Table 1, Table 2, and Table 3).

Table 1. Dynamic and Quasi-static Mechanical Properties of CWPs at Various Strain-Rates

Compos.	Matrix (%)	Strain-rate (/s)	σ_{UCS}[a] (MPa)	Specific Energy to Peak Load (kJ/kg)	MOR (MPa)	MOE (MPa)	Thk[b] (mm)	Density (Kg/m^3)
90%-PW	10	1000	504	17.54	19.4	3498	9.3	1188
	10	1400	254	15.19	19.4	3498	9.3	1188
	10	1600	295	19.24	19.4	3498	9.3	1188
85%-PW	15	1000	599	18.64	20.8	3997	8.9	1241
	15	1400	411	11.99	20.8	3997	8.9	1241
	15	1600	515	18.85	20.8	3997	8.9	1241
75%-PW	25	1000	452	13.09	25.1	4261	8.7	1272
	25	1400	486	15.87	25.1	4261	8.7	1272
	25	1600	655	17.09	25.1	4261	8.7	1272
50%-PW	50	1000	146	8.89	24.7	3922	8.3	1352
	50	1400	170	9.65	24.7	3922	8.3	1352
	50	1600	183	9.89	24.7	3922	8.3	1352
90%-Pine	10	1000	112	12.51	10.0	1836	10	1114
	10	1300	109	11.62	10.0	1836	10	1114
85%-Pine	15	1000	105	11.59	13.9	2507	9.5	1162
	15	1200	99	12.05	13.9	2507	9.5	1162
75%-Pine	25	1200	113	10.99	17.6	2978	8.8	1256
	25	1500	201	12.42	17.6	2978	8.8	1256
	25	1700	254	13.31	17.6	2978	8.8	1256
50%-Pine	50	1000	216	10.53	20.8	2958	8.2	1359
	50	1700	204	13.44	20.8	2958	8.2	1359
	50	1900	257	11.27	20.8	2958	8.2	1359
[a]Ultimate compressive strength; [b]Thickness								

Table 2. Pearson Correlation Coefficient Values for Dynamic, Flexural, and Dimensional Properties of PW CWPs [a]

Correlations:	Matrix (%)	Strain-rate (/s)	σ_{UCS}[b] (MPa)	Specific Energy to Peak Load (kJ/kg)	MOR (MPa)	MOE (MPa)	Thk[c] (mm)	Density (Kg/m^3)
Matrix (%)	--	0.000	-0.602*	-0.832*	0.783*	0.332	-0.945*	0.975*
Strain-rate	0.000	--	-0.079	0.135	0.000	0.000	0.000	0.000
Ultimate Compressive Strength (MPa)	-0.602*	-0.079	--	0.720*	-0.126	-0.400	0.374	-0.462
Specific Energy to Peak Load (kJ/kg)	-0.832*	0.135	0.720*	--	-0.583*	-0.189	0.764*	-0.799*
MOR	0.783*	0.000	-0.126	-0.583*	--	0.769*	-0.807*	0.839*
MOE	0.332	0.000	0.400	-0.189	0.769*	--	-0.603*	0.510
Thickness (mm)	-0.945*	0.000	0.374	0.764*	-0.870*	-0.603*	--	-0.993*
Density (Kg/m^3)	0.975*	0.000	-0.462	-0.799*	0.839*	0.510	-0.993*	--
[a]Values with asterisks were significant at $p = 0.05$								
[b]Ultimate compressive strength								
[c]Thickness								

Table 3. Pearson Correlation Coefficient Values for Dynamic, Flexural, and Dimensional Properties of Pine CWPs [a]

Correlations:	Matrix (%)	Strain-rate (/s)	σ_{UCS}[b] (MPa)	Specific Energy to Peak Load (kJ/kg)	MOR (MPa)	MOE (MPa)	Thk[c] (mm)	Density (Kg/m^3)
Matrix (%)	--	0.503	0.761*	-0.642*	0.925*	0.723*	-0.946*	0.974*
Strain-rate	0.503	--	0.736*	-0.158	0.535	0.489	-0.549	0.548
Ultimate Compressive Strength (MPa)	0.761*	0.736*	--	-0.107	0.776*	0.679*	-0.796*	0.802*
Specific Energy to Peak Load (kJ/kg)	-0.642*	-0.158	-0.107	--	-0.493	-0.283	0.513	-0.556
MOR	0.925*	0.535	0.776*	-0.493	--	0.931*	-0.996*	0.982*
MOE	0.723*	0.489	0.679*	-0.283	0.931*	--	-0.904*	0.851*
Thickness (mm)	-0.946*	-0.549	-0.796	0.513	-0.996*	-0.904*	--	-0.994*
Density (Kg/m^3)	0.974*	0.548	0.802*	-0.556	0.982*	0.851*	-0.994*	--

[a]Values with asterisks were significant at p = 0.05
[b]Ultimate compressive strength
[c]Thickness

Future studies will encompass wood panels made from other natural binders to compare with high strain-rate DDGS results, high strain-rate testing of individual components of each composite to obtain cause of strain-rate sensitivity, and computational modeling of high strain-rate material response.

CONCLUSIONS

1. At a strain-rate of approximately 1600/s, specimens with 75% paulownia wood (75%-PW) showed the highest ultimate strength and 90%-PW showed the highest specific energy of all composites.

2. Four variants of distiller's dried grains and solubles with paulownia wood (DDGS-PW) and DDGS-Pine composites illustrated the strain-rate sensitivity of wood composites made with DDGS binder. More investigation is needed to conclude the cause of the strain-rate sensitivity.

3. Wood composites made with 75%-PW exhibited the highest compressive strength, which illustrated that the fraction of bio-adhesive DDGS played a crucial role in the dynamic behavior and specific energy of the composites.

4. Based on energy absorption capacity, DDGS-PW bio-composites are more efficient for use in applications involving dynamic compression loading conditions.

5. In general, the specific energy and strength of panels made with Paulownia wood is higher than panels made with Pine.

bioresources.com

ACKNOWLEDGMENTS

REFERENCES CITED

American Conifer Society (ACS) (2019). "*Pinus strobus*/Eastern white pine," American Conifer Society, (https://conifersociety.org/conifers/pinus-strobus), Accessed 25 Aug 2019.

Allazadeh, M. R., and Wosu, S. N. (2011). "High strain rate compressive tests on wood," *Strain* 48(2), 101-107. DOI: 10.1111/j.1475-1305.2010.00802.x

Amaral-Labat, G. A., Pizzi, A., Goncalves, A. R., Celzard, A., Rigolet, S., and Rocha, G. J. M. (2008). "Environment-friendly soy flour-based resins without formaldehyde," *J. Appl. Polym. Sci.* 108(1), 624-632. DOI: 10.1002/app.27692

Cheesbrough, V., Rosentrater, K. A., and Visser, J. (2008). "Properties of distillers grains composites: A preliminary investigation," *J. Polym. Environ.* 16, 40-50. DOI: 10.1007/s10924-008-0083-x

DIN EN 310 (1993), "Wood-based panels: Determination of modulus of elasticity in bending and of bending strength," Deutsches Institut für Normung, Berlin, Germany.

Displays2GO (2019). "Comparing building materials: Particle board, MDF & plywood, Displays2Go," (https://www.displays2go.com/Guide/Comparing-Building-Materials-Particle-Board-MDF-Plywood-17), Accessed 30 Jan 2019.

Elias, P., and Boucher, D. (2014). *Planting for the Future: How Demand for Wood Products Could be Friendly to Tropical Forests*, Union of Concerned Scientists, Cambridge, MA, USA.

Frew, D. J., Forrestal, M. J., and Chen, W. (2002). "Pulse shaping techniques for testing brittle materials with a split Hopkinson pressure bar," *Experimental Mechanics* 42(1), 93-106. DOI: 10.1007/BF02411056

Frihart, C. R., and Birkeland, M. (2016). "Soy products for wood bonding," in: *Proceedings of the 59th International Convention of Society of Wood Science and Technology*, Curitiba, Brazil, pp. 192-199.

Ghahri, S., and Mohebby, B. (2017). "Soybean as adhesive for wood composites: Applications and properties," in: *Soybean: The Basis of Yield, Bio-mass and Productivity*, K. Minobu (ed.), Intech Publishing, London, UK, pp. 1-14.

Grand View Research (2018). *Wood Based Panel Market Size, Share & Trends Analysis Report by Product (Plywood, MDF, HDF, OSB, Particleboard, Hardboard), by Application (Furniture, Construction), by Region, and Segment Forecasts, 2018-2025* (GVR-2-68038-180-1), Grand View Research, San Francisco, CA, USA.

Green, D. W., Winandy, J. E., and Kretschmann, D. E. (1999). "Mechanical properties of wood," in: *Wood Handbook—Wood as an Engineering Material*, U.S. Department of Agriculture Forest Products Laboratory, Madison, WI, USA, pp. 4-1 to 4-46.

Hemmilä, V., Adamopoulos, S., Karlsson, O., and Kumar, A. (2017). "Development of sustainable bio-adhesives for engineered wood panels - A review," *RSC Adv.* 7(61), 38604-38630. DOI: 10.1039/c7ra06598a

Joshee, N. (2012). "Paulownia: A multipurpose tree for rapid lignocellulosic biomass production," in: *Handbook of Bioenergy Crop Plants*, C. Kole, C. P. Joshi, and D. R. Shonnard, D. (eds.), CRC Press, Boca Raton, FL, USA, pp. 671-686.

Kirker, G. T., Blodgett, A. B., Arango, R. A., Lebow, P. K., and Clausen, C. A. (2013). "The role of extractives in naturally durable wood species," *Int. Biodeter. Biodegrad.* 82, 53-58. DOI: 10.1016/j.ibiod.2013.03.007

Lang, S. M. (2012). *Design of a Split Hopkinson Bar Apparatus for use with Fiber Reinforced Composite Materials*, Master's Thesis, Utah State University, Logan, UT, USA.

Olson, J. R., and Carpenter, S. B. (1985). "Specific gravity, fiber length, and extractive content of young Paulownia," *Wood Fiber Sci.* 17(4), 428-438.

Pažitný, A., Boháček, Š., and Russ, A. (2011). "Application of distillery refuse in papermaking: novel methods of treated distillery refuse spectral analysis," *Wood Res.* 56(4), 533-544. DOI: Articles/4-20-140253. http://www.woodresearch.sk/articles/4-20-140253_09pazitny.pdf

Pettersen, R. C. (1984). "The chemical composition of wood," in: *The Chemistry of Solid Wood*, R. M. Rowell (ed.), American Chemical Society, Washington, D.C., USA, pp. 57-126.

Rencoret, J., Marques, G., Gutiérrez, A., Nieto, L, Jiménez-Barbero, J., Martínez, A. T., and Del Río, J. C. (2009). "Isolation and structural characterization of the milled-wood lignin from *Paulownia fortunei* wood," *Ind. Crop. Prod.* 30(1), 137-143. DOI: 10.1016/j.indcrop.2009.03.004

Sawyers, H. (2009). "FEMA's formaldehyde woes may change particleboard business," *Popular Mechanics*, (https://www.popularmechanics.com/home/how-to/a12199/4279057/), Accessed 27 Aug 2019.

Sutton, D. (2019). "Paulownia lumber: Properties of Paulownia wood," (https://paulowniasource.com/lumber), Accessed 5 March 2019.

Tisserat, B., Eller, F., and Harry-O'kuru, R. (2018a). "Various extraction methods influence the adhesive properties of dried distiller's grains and solubles, and press cakes of pennycress (*Thlaspi arvense* L.) and Lesquerella [*Lesquerella fendleri* (A. Gary) S. Watson] in the fabrication of lignocellulosic composites," *Fibers* 6(2), Article number 26. DOI: 10.3390/fib6020026

Tisserat, B. H., Wang, H.-S., Vaughn, S. F., Berhow, M. A., Peterson, S. C., Joshee, N., Vaidya, B. N., and Harry-O'Kuru, R. (2018b). "Fiberboard created using the natural adhesive properties of distillers dried grains with solubles," *BioResources* 13(2), 2678-2701. DOI: 10.15376/biores.13.2.2678-2701

Tisserat, B., Joshee, N. Mahapatra, A. K., Selling, G. W., and Finkenstadt, V. L. (2013a). "Physical and mechanical properties of extruded poly(lactic acid)-based *Paulownia elongata* biocomposites," *Ind. Crop Prod.* 44, 88-96. DOI: 10.1016/j.indcrop.2012.10.030

Tisserat, B., Reifschneider, L., Harry O'Kuru, R., and Finkenstadt, V. L. (2013b). "Mechanical and thermal properties of high-density polyethylene – dried distillers

grains with soluble composites," *BioResources* 8(1), 59-75. DOI: 10.15376/biores.8.1.59-75

Tisserat, B., Reifschneider, L., Joshee, N., and Finkenstadt, V. L. (2013c). "Properties of high-density polyethylene – Paulownia wood flour composites *via* injection molding," *BioResources* 8(3), 4440-4458. DOI: 10.15376/biores.8.3.4440-4458

Tsoumis, G. T. (2019). "Wood," *Encyclopedia Britannica*, (https://www.britannica.com/science/wood-plant-tissue), Accessed 18 June 2019.

U.S. Grains Council (USGC) (2017). *DDGS User Handbook 4th Edition*, U.S. Grains Council, Washington, D.C., USA.

Vnučec, D., Kutnar, A., and Goršek, A. (2016). "Soy-based adhesives for wood-bonding – A review," *J. Adhes. Sci. Technol.* 31(8), 910-931. DOI: 10.1080/01694243.2016.1237278

Wendel, G. W., and Smith, H. C. (1990). "Eastern white pine," U.S. Department of Agriculture, (https://www.srs.fs.usda.gov/pubs/misc/ag_654/volume_1/pinus/strobus.htm), Accessed 12 Jan 2020.

Widehammar, S. (2004). "Stress-strain relationships for spruce wood: Influence of strain rate, moisture content and loading direction," *Experimental Mechanics* 44(1), 44-48. DOI: 10.1007/BF02427975

Woodpansonline.com (2015). "MDF yearbook 2014/15: Global industry review," *Data Transcripts, Ltd.*, (http://www.woodpanelsonline.com/file-store/MDF_Yearbook_2015.pdf), Accessed 9 Dec 2019.

Yang, G., and Jaakkola, P. (2011). *Wood Chemistry and Isolation of Extractives from Wood Literature Study for BIOTULI Project*, Saimaa University of Applied Sciences, South Karelia, Finland.